Cardiff University School of Physics and Astronomy

MSc Research Project

Tidal Dwarf Galaxies In Nearby Interacting Systems

Navyasree Kovakkuni
Student Number: C1958765

Supervisor: Dr. Federico Lelli

18^{th} December, 2020

Contents

1 Introduction

Over the past few decades, there has been several studies conducted about star formation (SF) taking place at different locations in interacting systems. Most of these works concentrate on star formation in the inner regions, as galaxy mergers are known to trigger circum-nuclear starbursts. At the same time, SF is also found to occur at the outermost regions of such interacting systems, sometimes even 100 kpc away from the parent galaxies (Duc et al., 2006). Further studies on these regions revealed that most of the young stars found in them were born in-situ, out of pre-enriched gas from the parent galaxies. Intergalactic emission–line regions, Young (Super) Star clusters, and Tidal Dwarf Galaxies (TDGs) are some examples of such external star-forming regions (Duc et al., 2006). Even though SF is a fundamental astro-physical process that shapes galaxy formation and evolution, there are several aspects of it that remain to be fully understood (Kennicutt & Evans, 2012). TDGs, being identified as self-gravitating objects with in-situ star formation, can be used to understand the formation and evolution of galaxies, and also shine light on the process of SF. TDGs are dynamically young galaxies that share several properties with high redshift galaxies, such as very high gas fractions, absence of old stellar populations, and relatively turbulent gas disks, therefore studying them could enable us to understand how SF processes occurred at high redshifts (Braine et al., 2001). The Kennicutt-Schmidt law, also known as the the SF law, establishes a relation between the Star Formation Rate surface density (Σ_{SFR}) and gas surface density (Σ_{gas}) in star forming galaxies, at local scales SF can be considered to be driven by the physical processes occurring inside Giant Molecular Clouds (GMCs) and on global scales by large-scale gravitational instability. Since both processes contribute to the SF in galaxies, it is quite difficult to study and interpret SF law in them. The effects of DM in setting the disk stability can be isolated from other physical effects in TDGs since they lack a DM halo, making them good laboratories to conduct SF studies. This work aims to investigate the SF law in three sample TDGs, namely NGC 5291N, NGC 5291S and NGC 7252NW, and to compare the results with the SF law followed by normal galaxies.

2 Précis of Literature

2.1 Tidal Dwarf Galaxies

In 1951, Zwicky pointed out that during galaxy interactions clumps of gas and stars, stripped off from the spiral disks of the parent galaxies by tidal forces, could form self-gravitating objects are called TDGs and are found in the tidal tails of interacting systems. These objects known as TDGs have in-situ star formation, near solar metallicity and masses and sizes similar to dwarf galaxies (Duc et al., 2006). The first TDG to be reported was found at the southern tail of NGC4038/9 (Mirabel et al., 1992). Some of the main features of TDGs are the following:

- they have similar mass, size and SFRs as dwarf galaxies,
- they have higher metallicities than typical dwarf, as they are formed from pre-enriched materials, so they deviate from the mass-metallicity relation defined by "normal" galaxies (Duc et al., 2014),
- Baryons in the disk of interacting galaxies are segregated by the tidal forces from the dark matter (DM) in the halo. This occurs because the baryons in the disk, being dynamically cold, can form tails and evolve into a TDG, whereas the DM in the halo is dynamically hot and therefore cannot form narrow tails (Barnes & Hernquist, 1992; Elmegreen et al., 1993; Lelli et al., 2015). As a result TDGs are found to be devoid of a dominating dark matter halo,
- These stellar and gaseous condensations are self gravitating objects but are likely out of dynamical equilibrium, having a life time smaller than the dynamical orbital time (Lelli et al., 2015).

TDGs being devoid of non-baryonic DM should have a luminous mass similar to their dynamical mass (Duc, 2012) and as a result are being used to study the presence of baryonic DM (such as CO-dark molecular gas) in the disks of spiral galaxies (Duc et al., 2006). They are also used as laboratories to test the modified Newtonian dynamics (MOND) paradigm (Gentile et al., 2007). Several studies on TDGs (for example, Okazaki and Taniguchi, 2000, Bournaud and Duc, 2006) provides evidence to the tidal origin of some dwarf galaxies. TDGs are also found to have active star forming regions (Duc et al., 2006) and are being studied to test and understand different SF theories, mainly due to the following reasons:

- Their high metallicity makes it easier to detect and study molecular gas using CO emission lines in contrast to dwarf galaxies with low metallicities (Boquien et al., 2010).

- Since they are located far away from the disk, the on-going SF is not influenced directly by the self-gravity of the galactic disks apart from tidal forces (Boquien et al., 2007).
- TDGs could be used to understand a fundamental step in the SF process, the conversion of atomic hydrogen gas to molecular gas in gas clouds, which is still not fully understood (Braine et al., 2001).

2.2 Star Formation Law

SF is a key astro-physical process that plays a vital role in the study of interacting systems and galaxy evolution. In 1959 Schmidt put forth the star formation law in the Milky Way which relates the star formation rate (SFR) with gas density in units of volume density. This was later extended to external galaxies and modified in units of surface density by Kennicutt it is known as the Kennicutt-Schmidt law (or SF law) (Kennicutt, 1998a) and is given by:

$$\Sigma_{SFR} = A\,\Sigma_{gas}^{N} \tag{2.1}$$

where A and n are fitting parameters. In other words, the SF law gives a relation between the SFRs and the physical conditions existing in the interstellar medium (ISM) (Kennicutt, 1998a).

2.2.1 Star Formation Rate

SFR, the total mass of stars formed per year, depends upon different factors like the gas content, bar structure, mass and dynamical environment of a galaxy. Initially, evolutionary synthesis models of galaxy colors where used to derive SFRs, which have now been replaced by integrated light measurements in ultraviolet, far-infrared and nebular recombination lines (Kennicutt, 1998b). Emission lines are considered as a good probe for measuring SFRs as they are independent of star formation histories. This is due to the fact that the major contributors of the integrated ionizing flux are stars whose masses are greater than 10 $M_\odot$ and lifetimes less than 20 Myr. For this work we have used measurements from the Hα line to derive SFRs. Some of the other recombination lines that are also used to estimate SFRs are Hβ, Pα, Pβ, Brα and Brγ. Diffuse nebulae are considered as the place of origin of recombination lines of hydrogen, helium, nitrogen, neon, carbon etc. These nebulae are often accompanied by hot stars that radiates in UV, which in turn ionizes the gas within the nebulae giving rise to the emission lines during the recombination process. As these nebular emission lines re-emits the UV flux of O-B stars, they are used as a direct method to estimate the SFR (Kennicutt, 1998b). Hα derived SFR can be calculated using the following equation:

$$SFR = 7.9 \times 10^{-42}\, L(H\alpha) \tag{2.2}$$

where, SFR is in units of $M_\odot$ yr^{-1} and L(Hα) is the luminosity of Hα line in units of ergs s^{-1} (Kennicutt, 1998b). Equation 2.2 suggested by Kennicutt (1998b) assumes a Salpeter initial mass function (IMF) with a mass range of 0.1 $M_\odot$ to 100 $M_\odot$ and solar abundance. Apart from being highly sensitive to the assumed initial mass function (IMF), Hα derived SFRs are also prone to systematic errors due to extinction. For the purpose of this work we made use of the following nebular extinction ($A_{H\alpha}$) equation based on Balmer decrement as given in Bolatto et al., 2017:

$$A_{H\alpha} = 5.86\, log\, \frac{F_{H\alpha}}{2.86 F_{H\beta}} \tag{2.3}$$

where, $F_{H\alpha}$ and $F_{H\beta}$ are the integrated fluxes corresponding to Hα and Hβ profiles, respectively. The extinction corrected SFR can be calculated by revising Equation 2.2 to:

$$SFR = 7.9 \times 10^{-42}\, L(H\alpha) \times 10^{(A_{H\alpha}/2.5)} \tag{2.4}$$

2.2.2 Molecular Gas Tracer

One of the key process in SF is the condensation of clouds of atomic hydrogen, leading to its fragmentation, making the clouds denser and forming molecular gas, which then forms the stars (Braine et al., 2001). Consequently, molecular hydrogen (H_2), being the most abundant molecule, plays a vital role in SF and galaxy evolution. But due to its lack of permanent dipole moment, much of the H_2 in the clouds remains invisible (Bolatto et al., 2013; Kennicutt & Evans, 2012). Heavier elements like oxygen and carbon combine to form carbon monoxide (CO) under the conditions that exist within the molecular clouds. Due to its permanent dipole moment and low excitation energy, CO gets excited in the cold molecular clouds and emits radiation at a wavelength of 2.6 mm (Bolatto et al., 2013). For extragalactic studies, where it is difficult to resolve

the molecular gas clouds, the CO luminosity L(CO) corresponding to the emission as the molecule goes to a lower excitation level (rotational transition level, J = 0-1) is used to estimate the molecular gas mass (M_{mol}) (Kennicutt & Evans, 2012). The commonly employed method is to convert the integrated CO intensity, I(CO) to H_2 column density, N(H_2) by using the following equation:

$$N(H_2) = X(CO)\, I(CO) \tag{2.5}$$

where X(CO) is the CO to H_2 conversion factor (Kennicutt & Evans, 2012). .

$$M_{mol} = \alpha_{CO}\, L(CO) \tag{2.6}$$

Here α_{CO} is CO-to-H_2 conversion factor similar to X(CO) in Equation 2.5. In this work we have used equations from Bolatto et al. (2017) to convert the integrated CO flux to M_{mol}:

$$M_{mol} = 1.05 \times 10^4\, \frac{S_{CO}\Delta\nu\, D_L^2}{(1+z)} \tag{2.7}$$

where $S_{CO}\Delta\nu$ is the integrated CO flux in units of Jy km s^{-1}, D_L is the luminosity distance in units of Mpc and z is the redshift. Studies suggests that the values α_{CO} and X(CO) differs depending upon the region under study and the physical conditions (for example, Tacconi et al. (2008) and Meier et al. (2008)). For typical disk galaxies like the Milky Way, Bolatto et al. (2013) assumes X(CO) = 2 $\times 10^{20}$ cm^{-2} (K km $s^{-1})^{-1}$ and α_{CO} = 4.3 $M_\odot$ (K km s^{-1} $pc^{-2})^{-1}$. It is sensible to adopt the same conversion factor for TDGs since they retain the metallicity of the parent spiral galaxies.

3 Data

The three TDGs used in this work were chosen based on the availability of Hα and CO data cubes. The optical data for this project were obtained by using the Multi Unit Spectroscopic Explorer (MUSE), which is an integral field spectrograph installed on the fourth unit telescope (UT4) of the Very Large Telescope (VLT). The details of the observations made with MUSE are given in Table A.1. The CO (J=1-0) observations for the TDGs were made using the Atacama Large Millimeter/sub-millimeter Array (ALMA) on January 2016. All these data were received from Dr. Federico Lelli prior to the beginning of this work.

3.1 Samples

The three TDGs studied in this project are presented in Figure 3.1 along with VCC 2062, for which spatially resolved CO data were presented by Lisenfeld et al. (2016). The TDGs NGC 5291N and NGC 5291S are located in a system of two interacting galaxies, NGC 5291 and 'the Seashell'. Lying at the edge of the Abell 3574 cluster, this system of galaxies is surrounded by a large H I ring which is estimated to be formed 360 Myr ago due to a head-on collision. The collisional ring extends to a diameter of about 160 kpc and consists of many star forming regions (Lelli et al., 2015). NGC 5291N, NGC 5291S and NGC 5291SW are the largest star forming regions found in this system (see Figure 3.1). These three objects are found to have higher metallicities than dwarf galaxies of similar mass, which makes them bona-fide TDGs. NGC 7252NW is located at the edge of one of the two tidal tails of the merging system NGC 7252 (Boquien et al., 2010). This system of interacting galaxies, also called 'Atoms for Peace', is a classic example of a last stage of the 'Toomre Sequence' (Toomre et al., 1977) and is known to host two TDGs (Lelli et al., 2015). For NGC 5291SW and NGC 7252SE, CO data are not available and therefore are not studied in this work.

4 Methodology

The three main steps of this project were:

- Estimation of the SFRs for each of TDG using Hα and Hβ emission lines from MUSE observations,
- Estimation of the molecular gas mass for each TDG using CO (1-0) data from ALMA,
- Analysis and comparison of the SF law followed by TDGs with respect to normal galaxies.

What follows in this section is a detailed explanation of the steps involved in the estimation of the above parameters using the MUSE and ALMA data.

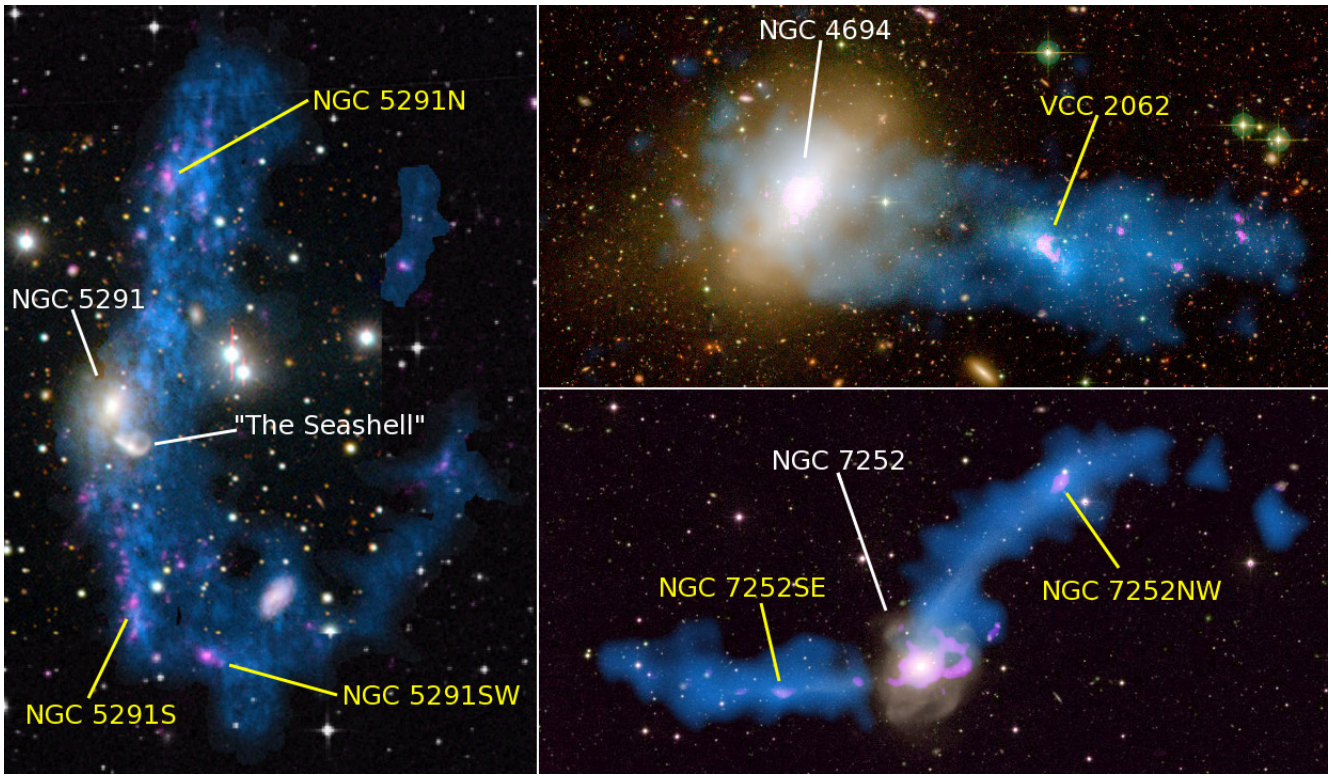

Figure 3.1: Optical images of three interacting systems overlaid with atomic hydrogen (HI) distribution and FUV emission.The pink colorscale shows the UV image (from GALEX) of the star forming region and the blue colorscale shows the HI emissions (from VLA). Left panel: interacting system NGC 5291 and 'the Seashell' galaxy along with three TDGs. Top right panel: disturbed lenticular galaxy NGC 4694 along with the TDG VCC 2062. Bottom right panel: The interacting system NGC 7252 along with the two TDGs (Lelli et al., 2015)

.

4.1 Estimating SFR

We used two different software, QFitsView [1] and Common Astronomy Software Applications (CASA) [2], to extract the integrated optical spectrum from the MUSE data cubes.

1. Integrated spectrum and area of choice: Once the data cube is loaded in the software, we have to define an area that covers the Hα emission to extract the integrated spectrum from the enclosed region. There are different approaches when it comes to choosing the area. Since studying SF law also requires molecular and atomic gas mass, one would have to retrieve integrated spectra from CO and HI data cubes as well. One approach is to choose the same area to estimate all the parameters so as to maintain consistency in the calculations. The disadvantage, however, is that Hα, CO, and especially HI emission can cover very different spatial areas, with HI emission being much more extended than the other two. Thus, the definition of a large common area may result in adding noise rather than signal to the integrated Hα and CO spectra. Another method is to define an area which would only cover the emission region that we are interested in. That is, for example, to define an area that covers only the region corresponding to Hα emission to estimate SFR and an area that covers only the region corresponding to CO emission to calculate the molecular gas mass. This method helps to restrict the calculations from having unwanted noise (when the defined area is too large) or to miss out the emissions from the required regions (when the defined area is too small). The extracted spectrum is then analysed using python to calculate different parameters.

2. Continuum subtraction: Emission spectra contain the continuum emission which occurs due to the combination of emissions from different blackbody emitters. It is a common practice to remove the continuum emission to isolate the flux from emission lines. The mean continuum flux was calculated and subtracted from the data considering two narrow spectral regions on either side of the profile. For example, in the case of NGC 5291N (see Figure 5.2) we considered the flux corresponding to the wavelength range 6642.12

[1] Available at: https://www.mpe.mpg.de/ ott/QFitsView/
[2] Available at: https://casa.nrao.edu/

$\AA$ to 6647.12 $\AA$ and 6647.12 $\AA$ to 664.62 $\AA$ to calculate the mean continuum flux and subtracted this value from the data. The same steps were followed to remove the continuum from the spectra of the other TDGs.

3. Flux calculation: The flux calculation was done by considering the Hα region from the integrated spectrum. Integrated Hα flux ($F_{H\alpha}$) was calculated using two methods:

   - Trapezoidal method: Trapezoidal rule is used in numerical analysis to calculate the area under a given curve by approximating the region to a trapezoid. In our analysis the total flux calculated using this method only considers the area under the Hα profile. This method does not depend on the line shape but requires a specific range for integration (the starting and ending wavelength of line emission) and therefore can be unreliable for spectra with low signal to noise ratio (S/N).
   - Curve fitting: The emission lines can often be described by a Gaussian profile due to line broadening, so we calculate the total flux by fitting a Gaussian to the region of interest. The area under the Gaussian curve then gives the integrated flux. This method would give inaccurate results if the line emission is not well described by a Gaussian.

   To estimate both the SFR and molecular gas mass we have to find the integrated flux from Hα and CO emission lines, respectively. The Hα emission lines are well described by a Gaussian curve (see Figure 5.1) and therefore we have used the curve fitting method to measure the total flux, whereas we used trapezoidal method to calculate the total flux for the CO emission lines as they do not exactly follow a Gaussian profile (see Figure 5.3).

4. Flux to luminosity conversion: $F_{H\alpha}$ have to be converted to luminosity in order to calculate the SFR. Luminosity can be calculated using:

$$L\,(\mathrm{ergs\,s^{-1}}) = 4\pi D_L^2 \times F_{H\alpha} \tag{4.1}$$

   where, D_L is the luminosity distance of the TDGs. We used the D_L values provided in Lelli et al. (2015).

5. Extinction correction and SFR: The SFR obtained from Equation 2.2 should be corrected for extinction. $F_{H\beta}$ was calculated from the integrated spectrum considering the region corresponding to Hβ emission, by following the same methods as that used for the calculation of $F_{H\alpha}$. For the given value of $F_{H\beta}$ we calculated the extinction and SFR using Equations 2.3 and 2.4, respectively. As can be seen from Figure 4.1 the region covered by Hβ emission is relatively small compared to the region enclosing Hα emission. Thus it would be unappropriate to extract the Hβ spectrum considering the same area as that of Hα emission because in doing so we would be integrating over spatial pixel that only contains noise. Therefore, we extracted the spectrum by identifying the area that contains Hβ emission and proceeded to calculate the total Hβ flux and extinction corrected SFR.

As mentioned, we carried out all the above steps using two software, QFitsView and CASA, considering areas based on HI emission (as given in Lelli et al. (2015)) and Hα emission. One of the drawbacks of using QFitsView is that it only allows the user to define a circular region to enclose the area of interest. But the Hα or Hβ emitting regions do not follow a circular shape (see Figure 4.1). Therefore,by defining a circular region to extract the integrated spectrum we are also including unwanted noise that does not contribute to Hα or Hβ emission. CASA on the other hand, provides an option to the user to choose between different shapes (like circle, ellipse, etc). In this work we have relied on the results obtained from our analysis using CASA, where we chose an elliptical area that encloses only region corresponding to Hα or Hβ emission.

4.2 Estimating Molecular Gas Mass

Molecular gas mass was obtained by extracting the integrated CO (1-0) spectrum using CASA .

1. Integrated CO line flux: To calculate the integrated CO line flux from the ALMA data cubes, we followed the same steps used to calculate $F_{H\alpha}$ (4.1). We considered only the spatial region around the CO emission line for calculations. The total CO line flux was calculated using both trapezoidal and curve fitting methods. The results discussed in section 5 are based on the estimates derived using trapezoidal method because the CO line profiles are not well described by a Gaussian.

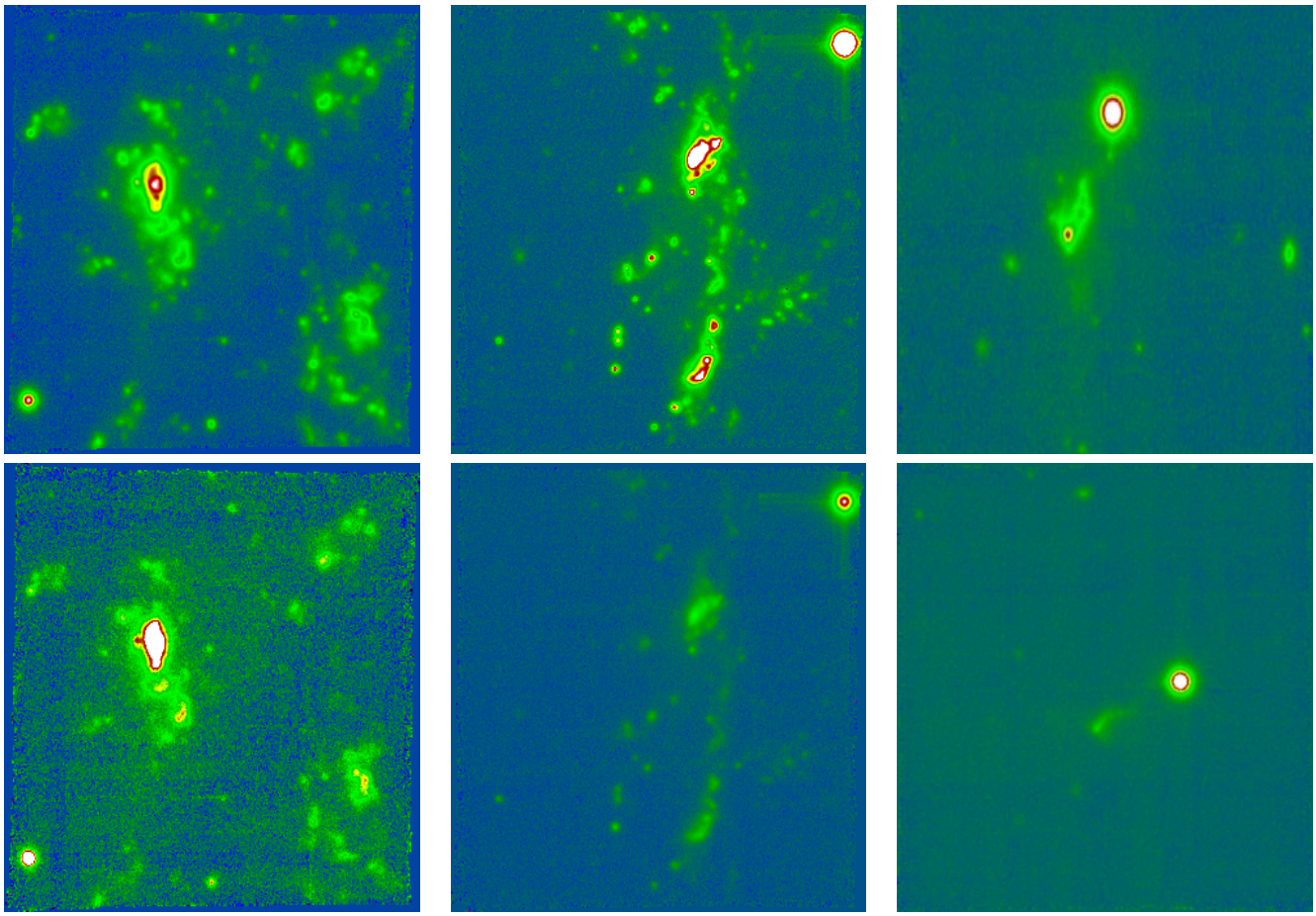

NGC 5291N NGC 5291S NGC 7252NW

Figure 4.1: The optical images (retrieved using QFitsView) of the TDGs obtained for a frequency range covering the Hα emission Hβ emission lines. Top panel: images displaying the Hα emission. Bottom panel: images displaying the Hβ emission.

2. Unit conversion: The total flux from the CO spectra is given in units of Jy beam^{-1} pixels km s^{-1}. Equation 2.7 requires flux in units of Jy km s^{-1}. In order to convert the flux to the required units we retrieved the values of BMAJ, BMIN, CDELT1 and CDELT2 from the fits header of each data cube. BMIN and BMAJ refer to the values of the minor and major axis of the beam in degrees, and CDELT1 and CDELT2 give the size of a pixel in degrees. We used the following equations to convert the units of flux to Jy km s^{-1}:

$$Number\ of\ pixels\ in\ a\ beam = \frac{BMAJ \times BMIN}{CDELT1 \times CDELT2} \tag{4.2}$$

$$Flux\ (\text{Jy km s}^{-1}) = \frac{Flux\ (\text{Jy beam}^{-1}\ \text{pixels km s}^{-1})}{Number\ of\ pixels\ in\ a\ beam} \tag{4.3}$$

3. Molecular gas mass: We calculated the redshift of each TDG by considering the central value of the Hα emission line. The molecular gas mass was estimated using Equation 2.7.

4.3 Generating Kennicutt-Schmidt Plot

The main aim of this project is to study the SF law followed by TDGs and compare the result with the SF law observed in normal galaxies. We used the data of 61 normal spiral galaxies published by Kennicutt (1998a) for comparison. The calibration used by Kennicutt (1998a) is based on Salpeter IMF, but our adopted calibration uses a Kroupa IMF (Kroupa, 2001). We made use of the scaling constant given by Kennicutt and Evans (2012) to rescale the SFRs from Kennicutt (1998a) SFR(K98) to a Kroupa IMF.

$$SFR_{corrected} = 0.68 \times SFR(K98) \tag{4.4}$$

To generate the Kennicutt-Schmidt diagram the SFRs and molecular gas masses were converted into units of surface density.

$$\Sigma_{SFR}\,(M_\odot\, yr^{-1}\, kpc^{-2}) = \frac{SFR}{Area} \tag{4.5}$$

$$\Sigma_{M_{mol}}\,(M_\odot\,pc^{-2}) = \frac{M_{mol}}{Area} \tag{4.6}$$

5 Results

5.1 Analysis of MUSE Data

All the results discussed in this section are based on the analysis of the data cubes using CASA and flux calculations using curve fitting method. The integrated spectrum was retrieved by defining an elliptical region, as an ellipse better defines the Hα and Hβ emission regions of the sample TDGs. As can be seen from Figure 5.1, the spectrum has a high signal to noise ratio and the Hα and Hβ profiles, are clearly detected. Moreover they are well described by a Gaussian (see Figures A.1 for NGC 5291S and A.2 for NGC 7252NW). The need

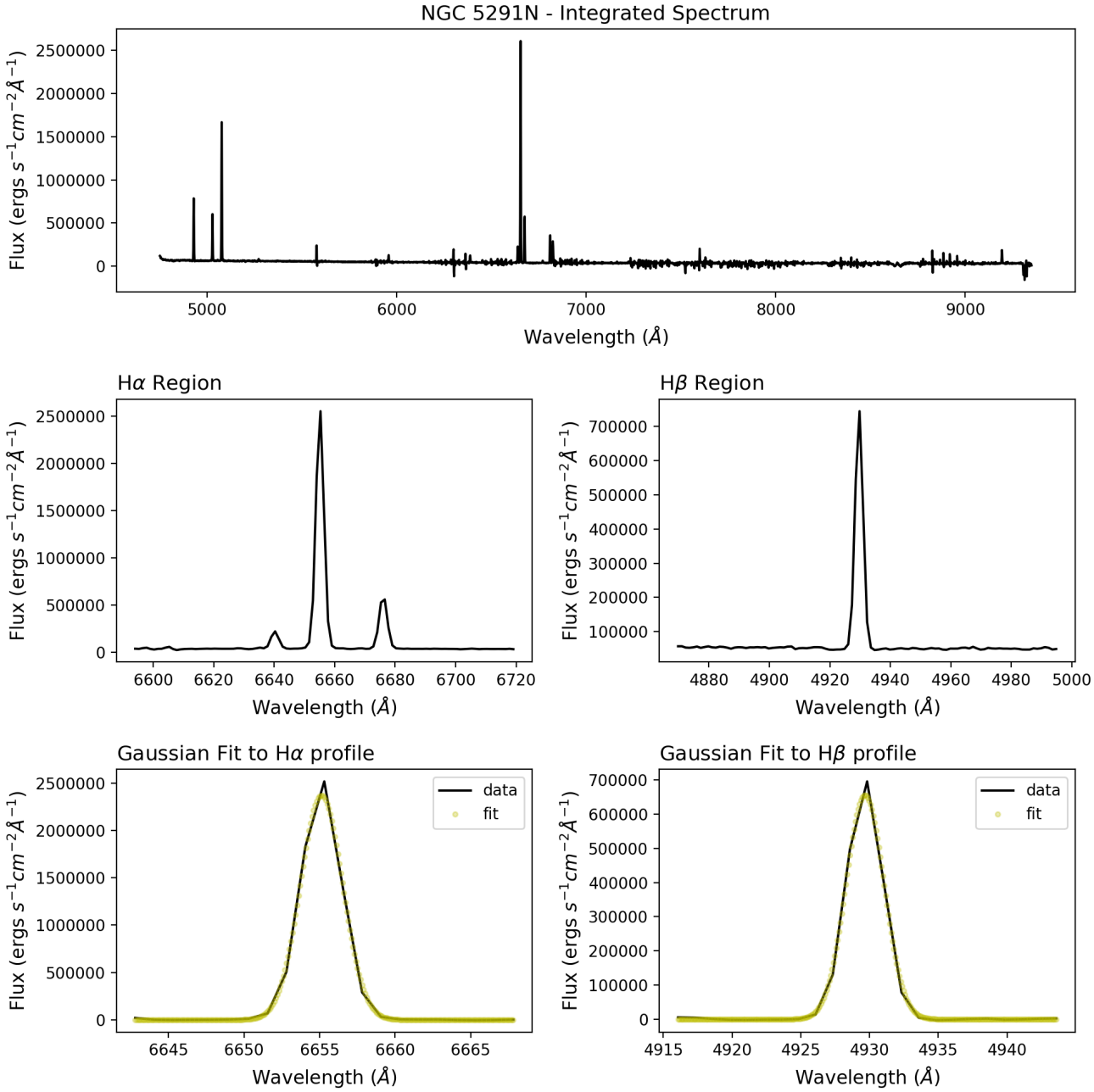

Figure 5.1: Analysis on the integrated optical spectrum of NGC 5291N. Top panel shows the integrated optical spectrum for NGC 5291N, middle panel displays the regions of interest for this work (Hα and Hβ) and the bottom panel shows the Gaussian fit performed over Hα and Hβ profile respectively.

to remove the stellar continuum from the data is clearly displayed in Figure 5.2. The data lies systematically above zero, whereas the Gaussian fit passes through zero. This offset was present in all spectra and therefore has been corrected by subtracting the continuum flux (see Table 5.1). The redshift and the systemic velocity

(v_{sys}) of the TDGs were estimated from the Doppler shift of Hα line using the equations:

$$z = \frac{\lambda_{observed} - \lambda_{rest}}{\lambda_{rest}} \tag{5.1}$$

$$v_{sys} = cz \tag{5.2}$$

where, $\lambda_{observed}$ is the observed wavelength of the Hα emission line, λ_{rest} is the rest wavelength of the Hα emission line and c is the velocity of light.The estimated values are given in Table 5.1.

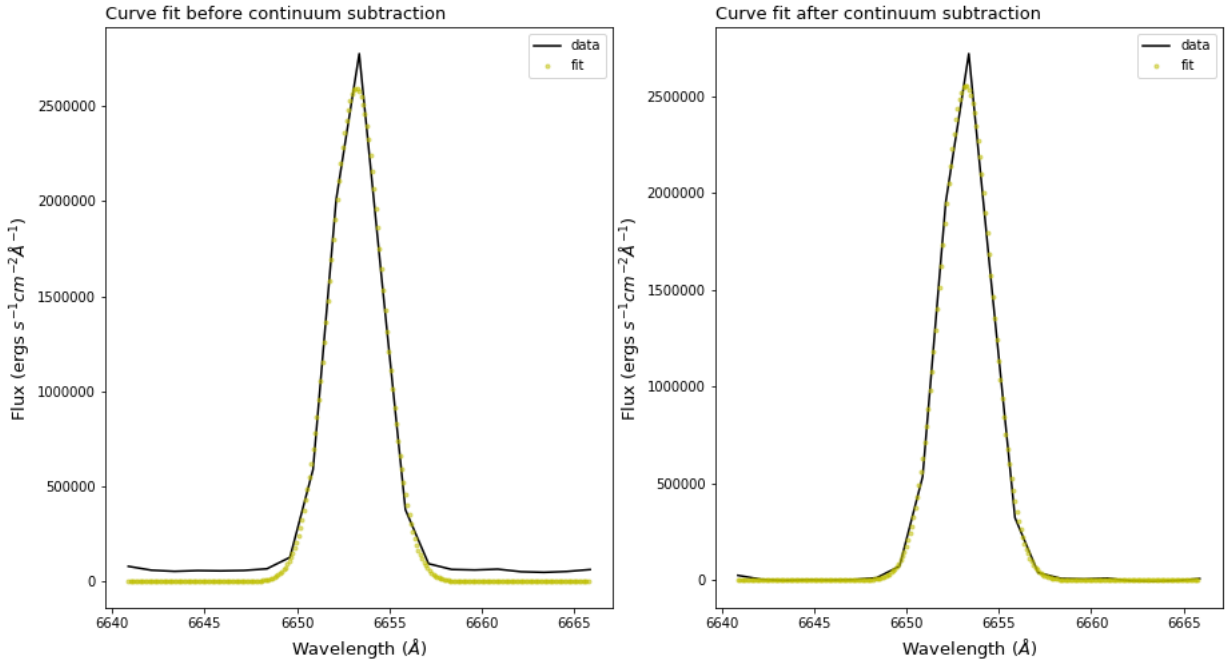

Figure 5.2: Curve fit performed on the Hα profile of NGC 5291N before and after continuum subtraction. As can be seen (from the left panel) there is an offset between the data and the fit on either side of the profile due to the presence of continuum emission in the spectrum. After the removal of continuum, both the data and the Gaussian passes through zero (right panel).

System	Mean continuum flux (for Hα profile) (ergs s^{-1} cm $^{-2}$)	Mean continuum flux (for Hβ profile) (ergs s^{-1} cm $^{-2}$)	z	V_{sys} (km/s)
NGC 5291N	36296.495	48700.780	0.014	4228.836
NGC 5291S	30158.962	38493.464	0.016	4780.396
NGC 7252NW	4902.336	5850.717	0.016	4771.579

Table 5.1: Mean continuum flux, redshift and systemic velocity calculated for the samples

System	Area (kpc^2)	$F_{H\alpha}$ (x10^{-14}) (ergs s^{-1} cm^{-2})	L (x10^{40}) (ergs s $^{-1}$)	SFR uncorr ($M_\odot\ yr^{-1}$)
NGC 5291N	29.701	8.278	3.808	0.301
NGC 5291S	44.152	5.203	2.394	0.189
NGC 7252NW	6.595	0.548	0.289	0.023

Table 5.2: Parameters measured using CASA

The parameters calculated from Hα profile are summarized in Table 5.2 while those from Hβ profile and corresponding extinction correction are given in Table 5.3. We find that the SFRs estimated in this work (see Table 5.3) are consistent with the results published by Boquien et al. (2010) using stellar synthesis models fitted to the spectral energy distribution of the same galaxies.

System	Area (kpc^2)	$F_{H\beta}$ ($x10^{-14}$) (ergs s^{-1} cm^{-2})	$A_{H\alpha}$	SFR corr ($M_\odot$ yr^{-1})
NGC 5291N	24.795	2.271	0.617	0.531
NGC 5291S	42.97	1.497	0.497	0.299
NGC 7252NW	3.873	0.121	1.176	0.068

Table 5.3: Estimations from Hβ emission line and extinction corrected SFRs

5.2 Analysis of ALMA Data

The same area used to estimate SFR (see Table 5.2) was used to retrieve the integrated spectra from CO data cubes. It can be seen from Figure 5.3 that the CO (1-0) emission line is not described by a Gaussian and that this data has a lower signal-to-noise ratio as compared to the data from the MUSE data cubes. For this reasons,

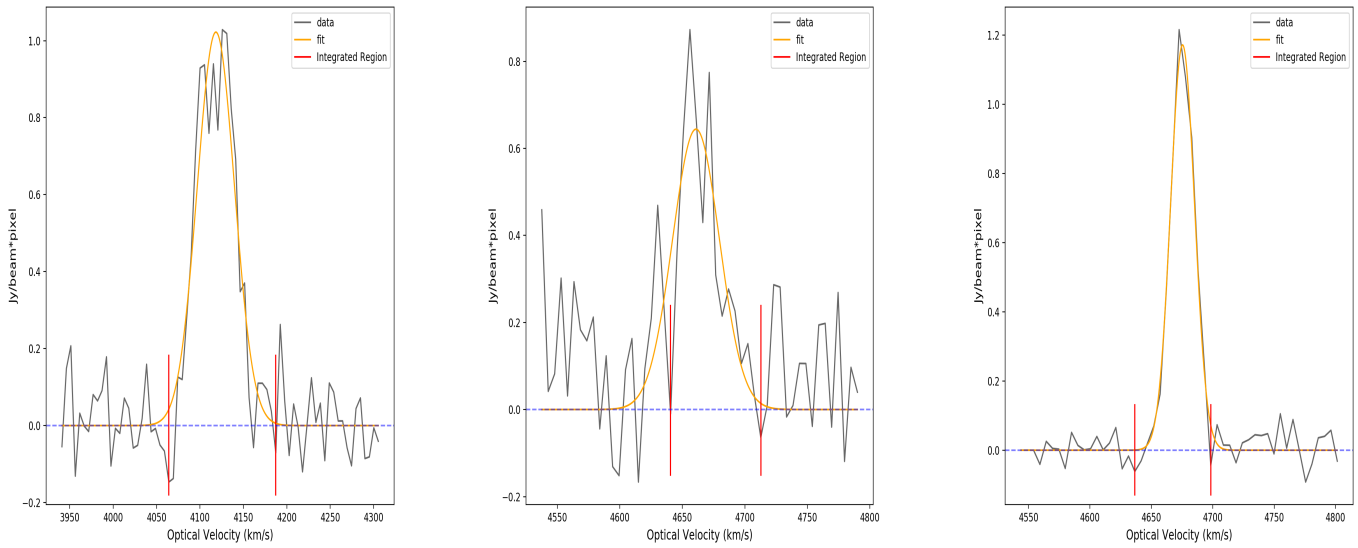

(a) NGC 5291N (b) NGC 5291S (c) NGC 7252NW

Figure 5.3: Integrated spectrum of the sample TDGs obtained from the CO cubes. The integrated region corresponds to the range over which the total flux was calculated using trapezoidal rule. The Gaussian fit is does not fully describe the observed emission profile.

the total CO flux calculated using trapezoidal method was used for further analysis. The results from curve fitting method are given in Table A.11. Table 5.4 gives the parameters used to convert the units of integrated flux, as mentioned in section 4.2.

System	BMAJ ($\times10^4$) (deg)	BMIN ($\times10^4$) (deg)	pixel size ($\times10^{-5}$) (deg)	rms Noise	Flux (Jy km/s)	S/N	M_{mol} ($x10^7$) ($M_\odot$)
NGC - 5291N	5.926	4.696	8.333	0.096	1.333	10.727	5.306
NGC - 5291S	5.897	5.075	8.333	0.166	0.600	5.256	2.384
NGC - 7252NW	7.431	4.394	8.333	0.047	0.596	26.048	2.723

Table 5.4: Parameters calculated from ALMA data

System	Area (kpc^2)	Σ_{SFR} ($M_\odot\ yr^{-1}$ kpc^{-2})	log Σ_{SFR} ($M_\odot\ yr^{-1}$ kpc^{-2})	$\Sigma_{M_{mol}}$ ($M_\odot$ pc^{-2})	log $\Sigma_{M_{mol}}$ ($M_\odot$ pc^{-2})
NGC 5291N	29.701	0.018	-1.748	1.786	0.252
NGC 5291S	44.152	0.007	-2.170	0.539	-0.268
NGC 7252NW	6.595	0.010	-1.989	4.128	0.616

Table 5.5: Surface densities of SFR and molecular gas mass from analysis with CASA

5.3 Kennicutt-Schmidt Diagram

In this work, we have retrieved the integrated spectrum and estimated the SFRs using different methods. The different methods provide similar results for NGC 5291N and NGC 5291S (within a factor of two), but very different results for NGC 7252NW (see Table A.10) because the Hα emission in this object appears to be significantly extincted, so the area used to extract the weak Hβ line is crucial. In general, the SFR surface density considering HI area is lower than considering Hα area because the SFR is divided by a larger number. Therefore, we consider the CASA-based extraction as the most trustworthy one. Figure 5.4 shows the relationship between the SFR surface density and molecular gas density of the TDGs in comparison with the relation followed by 61 normal spiral galaxies. We see that the TDGs lies along the SF law defined by normal spiral galaxies and they lie above the star burst region, indicating on going SF. Figure 5.4 also shows the weak correlation between the Hα derived SFRs and $\Sigma_{M_{mol}}$ as was reported by Kennicutt (1998a).

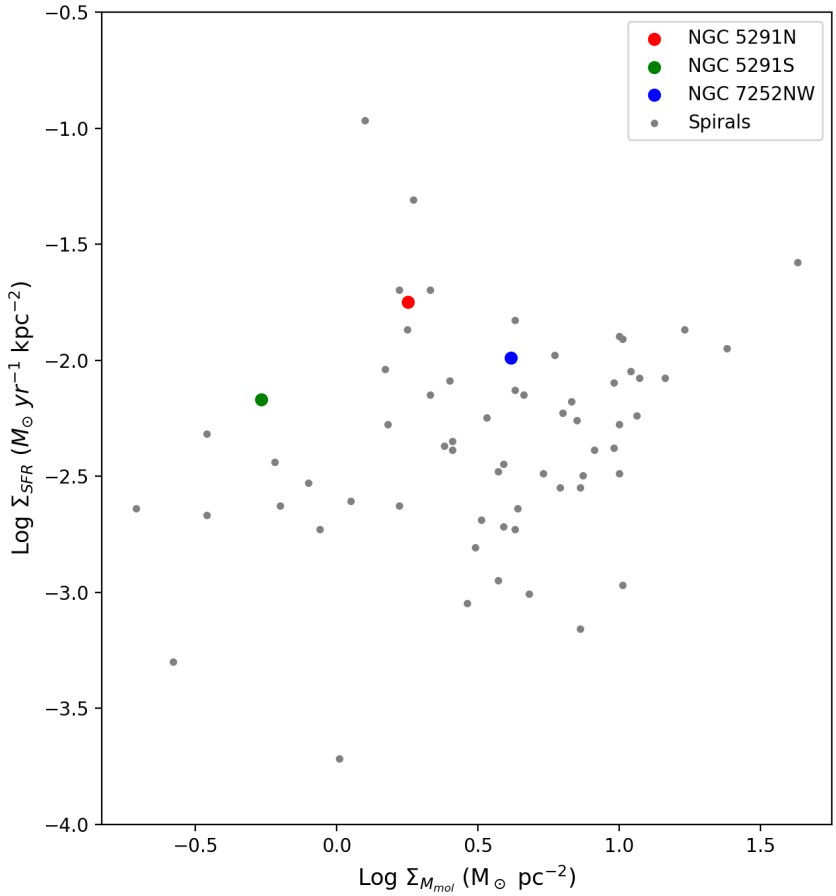

Figure 5.4: Kennicutt-Schmidt Diagram for the TDG samples plotted over normal spiral galaxies (Kennicutt, 1998a).

6 Conclusions

We studied the SF law followed by three bona-fide TDGs, NGC 5291N, NGC 5291S and NGC 7252NW by using Hα and CO data cubes from MUSE and ALMA, respectively. We analysed the data cubes using CASA and estimated the SFR and molecular mass of the sample. Our main conclusions can be summarized as follows:

1. Comparing the SFR obtained from the two softwares, CASA and QFitsView (see Table A.10) we notice that the choice of the software doesn't make a difference.

2. The extinction of NGC 7252NW is quite high irrespective of the method. This could possibly be because of the high dust content in the TDG.

3. The molecular gas density that we calculated seems to differ by several orders when compared to other studies like Lelli et al. (2015) and Braine et al. (2001) which are based on observations from single-dish telescopes. This difference could possibly be due to a substantial amount of diffuse CO which was filtered by the ALMA observations but probed by the single-dish observation. This could happen because interferometers probe only the more dense and compact emission and may miss the diffuse CO flux. A recent study by Querejeta et al. (2020) on another TDG, J1023+1952 found the presence of huge amount of diffuse CO which was missed by the interferometer as these were not from high-density CO and/or GMCs.

4. The Kennicutt-Schmidt diagram shows that the TDGs follow the same SF law as the normal spiral galaxies even though the SF occurs in a very different environment. Works published by Lisenfeld et al. (2016) on the TDG VCC 2062 also suggests a similar result.

5. We also find that the TDGs lie at the upper boundary of the SF relation, in the star burst region, indicating that the TDGs are forming stars with high efficiencies. Similar results were found by Fensch et al. (2019) about the young clusters in the TDGs in the collisional ring of NGC 5291. The star cluster forming efficiency estimated for the TDGs in this system were observed to be similar to that of blue compact dwarf galaxies (which are star bursting galaxies). This finding contradicts the theory that the low-metallicity environment acts as a good ground for star cluster formation.

Some of the possible future work would be:

- Study the SF law using the total gas density, which would require the estimation of atomic gas mass from HI data cubes. This result could then be compared with SF law followed by normal spiral galaxies.

- The presence of diffuse CO could be confirmed by overlaying the CO spectra from single dish Observations.

- Further studies with other bona-fide TDGs would help to confirm whether the TDGs follow same SF law as spiral galaxies. If they do, then TDGs can be used as good laboratories to study and understand SF process that could have taken place in the early universe.

7 Critique of Project

Prior to the start of the project, as preliminary work I recreated the plots from de los Reyes and Kennicutt Jr (2019) in order to get an understanding about how the SF law is being studied. This step had a purely didactic purpose, work mentioned above made use of UV derived SFRs and for my project I was using Hα emission line to derive SFRs, so comparing them would be complicated and potentially prone to observational biases. Nevertheless, this pre-work helped me to understand the procedure that is in general followed in SF studies, the variant forms of SF law that are being tested in different environments, and how the SFRs derived using different probes would vary. Moreover, I was able to learn how mathematical procedures like least squares fit, orthogonal distance regression, etc., are being utilised to test and study scientific laws. The work carried

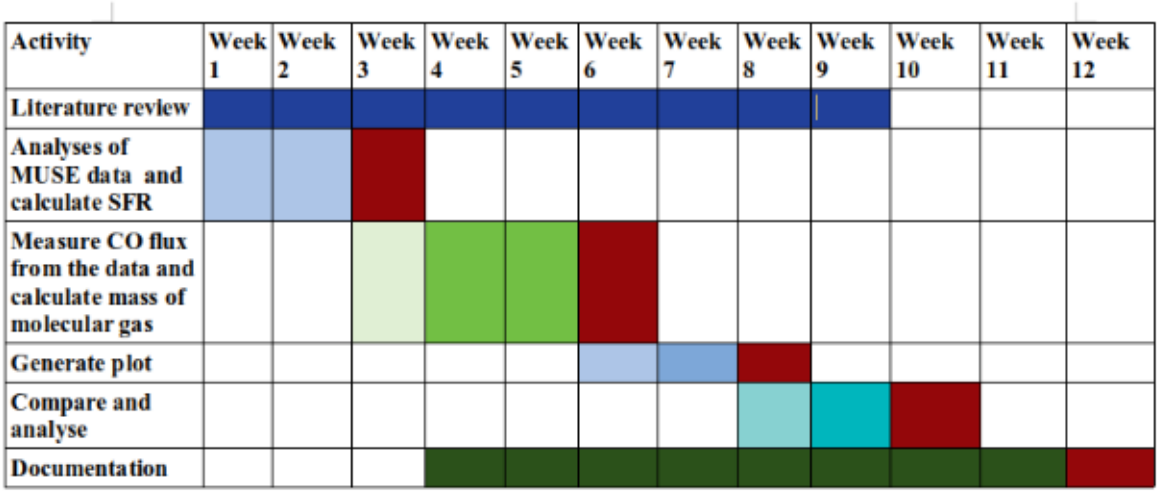

Figure 7.1: Gantt chart demonstrating the project timeline. The red blocks represents the proposed deadline for the activity and each color represent a different activity with the lighter shades indicating a earlier start period for the activity.

out didn't deviate from the project objectives and plans that were described in the proposal. Considering the timeline, (Figure7.1) I would say that the the project didn't fall along the timeline that was proposed. The first two weeks of the project went along as was planned; getting to understand and working with the software and conducting the literature review. In the proposal extra time was allocated for understanding how to use the software, which wasn't actually required as this work required me to only use these software to retrieve the spectrum and not to conduct further analysis, which was done using python. The step that actually consumed time, which wasn't accounted for in the proposal, was the analysis of the MUSE data using python. It took almost four weeks to develop a python script for the entire analysis of the MUSE data. One reason for this was that I was not certain about the steps involved in estimating the SFRs during the initial week. Most of the methods was a chosen with trial and error which consumes time as well. I would say that I had not overlooked to the fact that the project would progress with trail and error in the choice of area in the research proposal. Even though the analysis with MUSE data took longer than was anticipated, it didn't tamper the overall timeline of the project, since the python script that was developed at this stage was utilised for all the other analysis going forward. Once I had the script ready with all the improvements I was able to complete the the rest of the analysis on time.

The major issue that I had to encounter in between the project would be with the system failure. I run into issues with Ubuntu installation in my laptop twice during the course of the project. I was able to re-install Ubuntu and recover my files the first time but wasn't able to recover the installation or re-install Ubuntu for the second time, which happened two weeks before the submission date. Because of the same I had to drop two analysis: the consistency check with CO single dish spectra and estimation of the atomic gas mass, as the software I used only works in linux based systems and Mac OS. As these two analysis weren't a part of the proposed project this hasn't led to any deviation from the submitted plan. Even though these weren't in the initially proposed work, it would have been really good to include these results so as to support the conclusions. Some of the key takeaway points would be:

- To start working on the thesis mid-way through the project and not to drag this step towards the end.

- To make sure that you have access to proper working computers (albeit the current pandemic situation with home working and limited IT support has exacerbated this situation)
- Not to get too much focussed on the analysis, writing the thesis is also an important part

One of the major drawbacks with the proposed project plan was that it was solely based on the major milestones in the project, like estimating the SFRs and molecular gas mass, and didn't take into account the sub-steps involved in reaching these milestones. Keeping a project diary along with the summary of all the meetings and discussions with the supervisor has helped with writing the thesis. Having regular meetings and discussions with the supervisor was quite beneficial for the project.

References

Barnes, J. E. & Hernquist, L. (1992). Formation of dwarf galaxies in tidal tails. *Nature*, *360*(6406), 715–717.

Bolatto, A. D., Wolfire, M. & Leroy, A. K. (2013). The co-to-h2 conversion factor. *Annual Review of Astronomy and Astrophysics*, *51*, 207–268.

Bolatto, A. D., Wong, T., Utomo, D., Blitz, L., Vogel, S. N., Sánchez, S. F., Barrera-Ballesteros, J., Cao, Y., Colombo, D., Dannerbauer, H. et al. (2017). The edge-califa survey: Interferometric observations of 126 galaxies with carma. *The Astrophysical Journal*, *846*(2), 159.

Boquien, M., Duc, P.-A., Braine, J., Brinks, E., Lisenfeld, U. & Charmandaris, V. (2007). Polychromatic view of intergalactic star formation in ngc 5291. *Astronomy & Astrophysics*, *467*(1), 93–106.

Boquien, M., Duc, P.-A., Galliano, F., Braine, J., Lisenfeld, U., Charmandaris, V. & Appleton, P. (2010). Star formation in collision debris: Insights from the modeling of their spectral energy distribution. *The Astronomical Journal*, *140*(6), 2124.

Bournaud, F. & Duc, P.-A. (2006). From tidal dwarf galaxies to satellite galaxies. *Astronomy & Astrophysics*, *456*(2), 481–492.

Braine, J., Duc, P.-A., Lisenfeld, U., Charmandaris, V., Vallejo, O., Leon, S. & Brinks, E. (2001). Abundant molecular gas in tidal dwarf galaxies: On-going galaxy formation. *Astronomy & Astrophysics*, *378*(1), 51–69.

de los Reyes, M. A. & Kennicutt Jr, R. C. (2019). Revisiting the integrated star formation law. i. non-starbursting galaxies. *The Astrophysical Journal*, *872*(1), 16.

Duc, P.-A. (2012). Birth, life and survival of tidal dwarf galaxies. *Dwarf galaxies: Keys to galaxy formation and evolution* (pp. 305–313). Springer.

Duc, P.-A., Bournaud, F. & Boquien, M. (2006). Tidal dwarf galaxies as laboratories of star formation and cosmology. *Proceedings of the International Astronomical Union*, *2*(S237), 323–330.

Duc, P.-A., Paudel, S., McDermid, R. M., Cuillandre, J.-C., Serra, P., Bournaud, F., Cappellari, M. & Emsellem, E. (2014). Identification of old tidal dwarfs near early-type galaxies from deep imaging and h i observations. *Monthly Notices of the Royal Astronomical Society*, *440*(2), 1458–1469.

Elmegreen, B., Kaufman, M. & Thomasson, M. (1993). An interaction model for the formation of dwarf galaxies and 10 exp 8 solar mass clouds in spiral disks. *The Astrophysical Journal*, *412*, 90–98.

Fensch, J., Duc, P.-A., Boquien, M., Elmegreen, D. M., Elmegreen, B. G., Bournaud, F., Brinks, E., de Grijs, R., Lelli, F., Renaud, F. et al. (2019). Massive star cluster formation and evolution in tidal dwarf galaxies. *Astronomy & Astrophysics*, *628*, A60.

Gentile, G., Famaey, B., Combes, F., Kroupa, P., Zhao, H. & Tiret, O. (2007). Tidal dwarf galaxies as a test of fundamental physics. *Astronomy & Astrophysics*, *472*(2), L25–L28.

Kennicutt, R. C. (1998a). The global schmidt law in star-forming galaxies. *The Astrophysical Journal*, *498*(2), 541.

Kennicutt, R. C. (1998b). Star formation in galaxies along the hubble sequence. *Annual Review of Astronomy and Astrophysics*, *36*(1), 189–231.

Kennicutt, R. C. & Evans, N. J. (2012). Star formation in the milky way and nearby galaxies. *Annual Review of Astronomy and Astrophysics*, *50*, 531–608.

Kroupa, P. (2001). On the variation of the initial mass function. *Monthly Notices of the Royal Astronomical Society*, *322*(2), 231–246.

Lelli, F. et al. (2015). Gas dynamics in tidal dwarf galaxies: Disc formation at z= 0. *Astronomy & Astrophysics*, *584*, A113.

Lisenfeld, U., Braine, J., Duc, P., Boquien, M., Brinks, E., Bournaud, F., Lelli, F. & Charmandaris, V. (2016). Molecular gas and star formation in the tidal dwarf galaxy vcc 2062. *Astronomy & Astrophysics*, *590*, A92.

Meier, D. S., Turner, J. L. & Hurt, R. L. (2008). Nuclear bar catalyzed star formation: 13co, c18o, and molecular gas properties in the nucleus of maffei 2. *The Astrophysical Journal*, *675*(1), 281.

Mirabel, I. F., Dottori, H. A. & Lutz, D. (1992). Genesis of a dwarf galaxy from the debris of the antennae. *Astronomy and Astrophysics. Berlin. Vol. 256, no. 1 (Mar. 1992), p. l19-l22.*

Okazaki, T. & Taniguchi, Y. (2000). Dwarf galaxy formation induced by galaxy interactions. *The Astrophysical Journal*, *543*(1), 149.

Querejeta, M., Lelli, F., Schinnerer, E., Colombo, D., Lisenfeld, U., Mundell, C., Bigiel, F., Garcıa-Burillo, S., Herrera, C., Hughes, A. et al. (2020). Alma resolves giant molecular clouds in a tidal dwarf galaxy. *arXiv preprint arXiv:2011.01287*.

Tacconi, L., Genzel, R., Smail, I., Neri, R., Chapman, S., Ivison, R., Blain, A., Cox, P., Omont, A., Bertoldi, F. et al. (2008). Submillimeter galaxies at z$\tilde{2}$: Evidence for major mergers and constraints on lifetimes, imf, and co-h2 conversion factor. *The Astrophysical Journal*, *680*(1), 246.

Toomre, A., Tinsley, B. & Larson, R. (1977). Evolution of galaxies and stellar populations. *Proceedings of a Conference at Yale University, May*, 19–21.

A Appendix

A.1 Tables

System	Date of Observation (dd-mm-yyyy)	Spectral Range (Å)	Telescope Used	Focal Length (m)
NGC 5291 N	26-06-2014	4749.622–9349.622	ESO-VLT-U4	121.561
NGC 5291S	22-01-2018	4600.435-9350.435		
NGC 7252NW	16-07-2017	4600.242-9350.242		

Table A.1: Details of Optical observations made with MUSE

System	Distance (Mpc)	Radius (as given in Lelli et al., 2015) (kpc)	Radius (pixels)
NGC 5291N	62	4.8	80
NGC 5291S	62	7.2	120
NGC 7252NW	66.5	7.7	120

Table A.2: Radius used to extract the spectrum based on HI emission

System	Area considered for Hα (kpc^2)	F$_{H\alpha}$ (x10^{-14}) (ergs s^{-1} cm^{-2})	Area considered for Hβ (kpc^2)	F$_{H\beta}$ (x10^{-14}) (ergs s^{-1} cm^{-2})
NGC 5291N	70.677	8.915	27.608	2.292
NGC 5291S	159.022	6.652	89.450	1.736
NGC 7252NW	182.577	0.645	7.924	0.146

Table A.3: Parameters measured using QFitsView based on HI emission area

System	L (x10^{40}) (ergs s $^{-1}$)	SFR uncorr ($M_\odot\ yr^{-1}$)	Extinction	SFR corr ($M_\odot\ yr^{-1}$)
NGC 5291N	4.101	0.324	0.783	0.666
NGC 5291S	3.060	0.242	0.744	0.480
NGC 7252NW	0.341	0.027	1.106	0.075

Table A.4: Parameters derived using QFitsView based on HI emission area

System	Area considered for Hα (kpc^2)	F$_{H\alpha}$ (x10^{-14}) (ergs s^{-1} cm^{-2})	Area considered for Hβ (kpc^2)	F$_{H\beta}$ (x10^{-14}) (ergs s^{-1} cm^{-2})
NGC 5291N	39.756	8.436	27.608	2.292
NGC 5291S	110.432	6.170	89.450	1.736
NGC 7252NW	20.286	0.615	7.924	0.146

Table A.5: Parameters measured using QFitsView based on area that covers Hα emission alone

System	L (x10^{40}) (ergs s $^{-1}$)	SFR uncorr ($M_\odot\ yr^{-1}$)	Extinction	SFR corr ($M_\odot\ yr^{-1}$)
NGC 5291N	3.881	0.307	0.642	0.554
NGC 5291S	2.838	0.224	0.553	0.373
NGC 7252NW	0.326	0.026	0.988	0.064

Table A.6: Parameters derived using QFitsView based on area that covers Hα emission alone

System	Software used	Area based on	Mean continuum flux (ergs s^{-1} cm^{-2})
NGC 5291N	QFitsView	HI emission	56148.964
	QFitsView	Hα emission	41398.179
	CASA	Hα emission	36296.495
NGC 5291S	QFitsView	HI emission	51290.137
	QFitsView	Hα emission	40608.402
	CASA	Hα emission	30158.962
NGC 7252NW	QFitsView	HI emission	24927.939
	QFitsView	Hα emission	8797.644
	CASA	Hα emission	4902.336

Table A.7: Mean continuum flux calculated for the samples in all three analysis

System	Software used	Area (kpc^2)	$F_{H\alpha}$ (ergs s^{-1} cm^{-2})	SFR corr ($M_\odot$ yr^{-1})
NGC 5291N	QFitsView	70.677	8.934	0.676
	QFitsView	39.756	8.451	0.561
	CASA	29.701	8.292	0.539
NGC 5291S	QFitsView	159.022	6.721	0.499
	QFitsView	110.432	6.229	0.387
	CASA	44.152	5.231	0.311
NGC 7252NW	QFitsView	182.577	0.643	0.077
	QFitsView	20.286	0.614	0.066
	CASA	6.595	0.546	0.069

Table A.8: SFR estimated using trapezoidal method

System	Software used	Area (kpc^2)	$F_{H\beta}$ (ergs s^{-1} cm^{-2})	Extinction (A)
NGC 5291N	QFitsView	27.608	2.284	0.796
	QFitsView	27.608	2.284	0.655
	CASA	29.701	2.263	0.617
NGC 5291S	QFitsView	89.450	1.732	0.776
	QFitsView	89.450	1.732	0.583
	CASA	44.152	1.483	0.533
NGC 7252NW	QFitsView	7.924	0.144	1.141
	QFitsView	7.924	0.144	1.026
	CASA	6.595	0.119	1.203

Table A.9: Extinction values estimated using trapezoidal rule.

	QFitsView	Hα emission	Trapezoidal Rule	0.561	0.014
			Curve Fitting	0.554	0.014
	CASA	Hα emission	Trapezoidal Rule	0.539	0.018
			Curve Fitting	0.531	0.018
NGC 5291S	QFitsView	HI emission	Trapezoidal Rule	0.499	0.003
			Curve Fitting	0.480	0.003
	QFitsView	Hα emission	Trapezoidal Rule	0.387	0.004
			Curve Fitting	0.373	0.003
	CASA	Hα emission	Trapezoidal Rule	0.311	0.007
			Curve Fitting	0.299	0.007
NGC 7252NW	QFitsView	HI emission	Trapezoidal Rule	0.077	0.0004
			Curve Fitting	0.075	0.0004
	QFitsView	Hα emission	Trapezoidal Rule	0.066	0.003
			Curve Fitting	0.064	0.003
	CASA	Hα emission	Trapezoidal Rule	0.069	0.010
			Curve Fitting	0.068	0.010

Table A.10: Comparison between SFRs estimated using trapezoidal method and curve fitting.

System	Flux (Jy km/s)	M_{mol} ($\times 10^7$) $M_\odot$	$\Sigma_{M_{mol}}$ ($M_\odot$ pc^{-2})	log $\Sigma_{M_{mol}}$ ($M_\odot$ pc^{-2})
NGC 5291N	1.374	5.468	1.841	0.265
NGC 5291S	0.702	2.796	0.633	-0.198
NGC 7252NW	0.609	2.426	3.678	0.566

Table A.11: Parameters estimated from AlMA data using curve fit method.

A.2 Figures

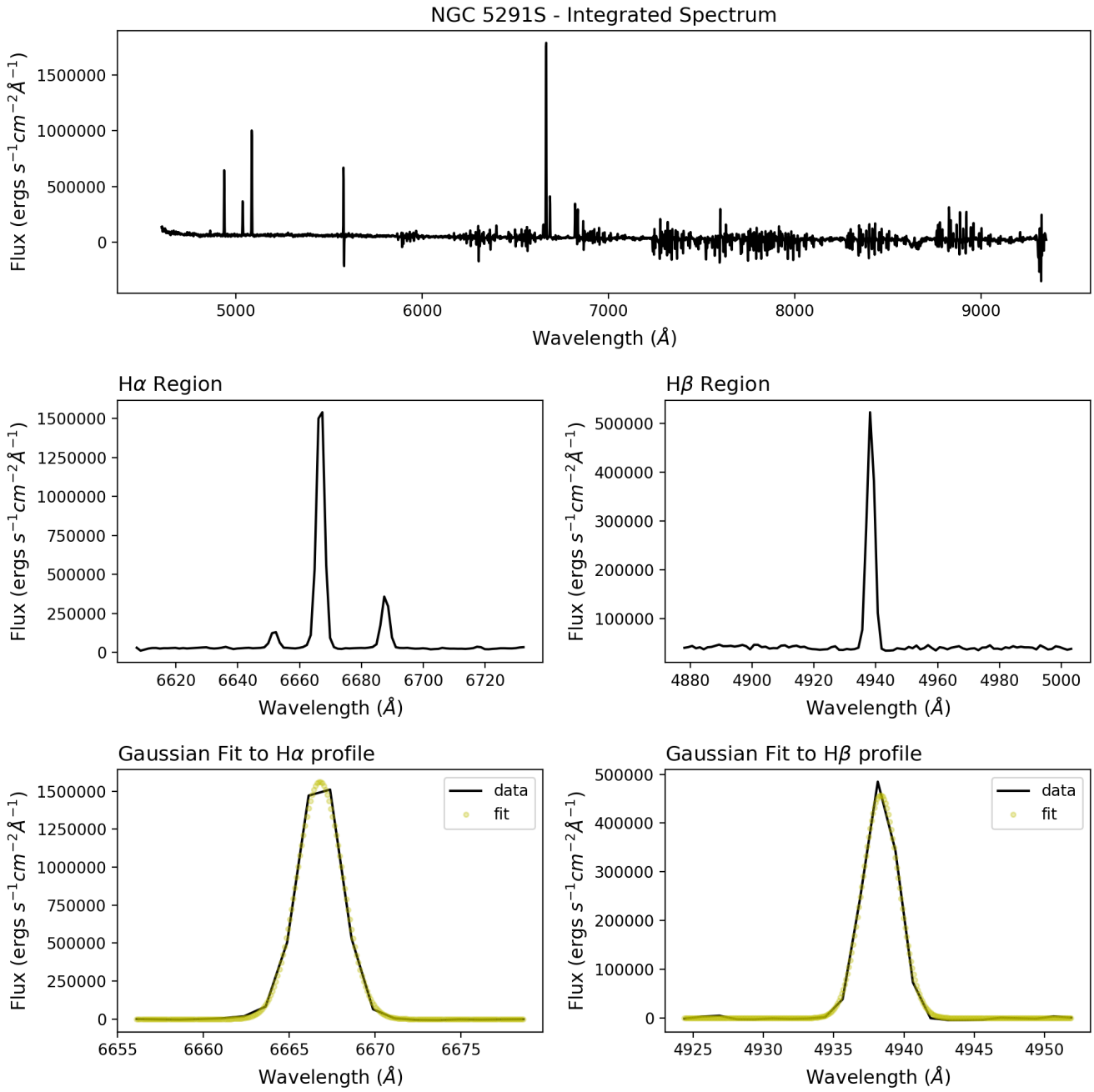

Figure A.1: Analysis on the integrated optical spectrum of NGC 5291S. Top panel shows the integrated optical spectrum for NGC 5291S, middle panel displays the regions of interest for this work (Hα and Hβ) and the bottom panel shows the Gaussian fit performed over Hα and Hβ profile, respectively.

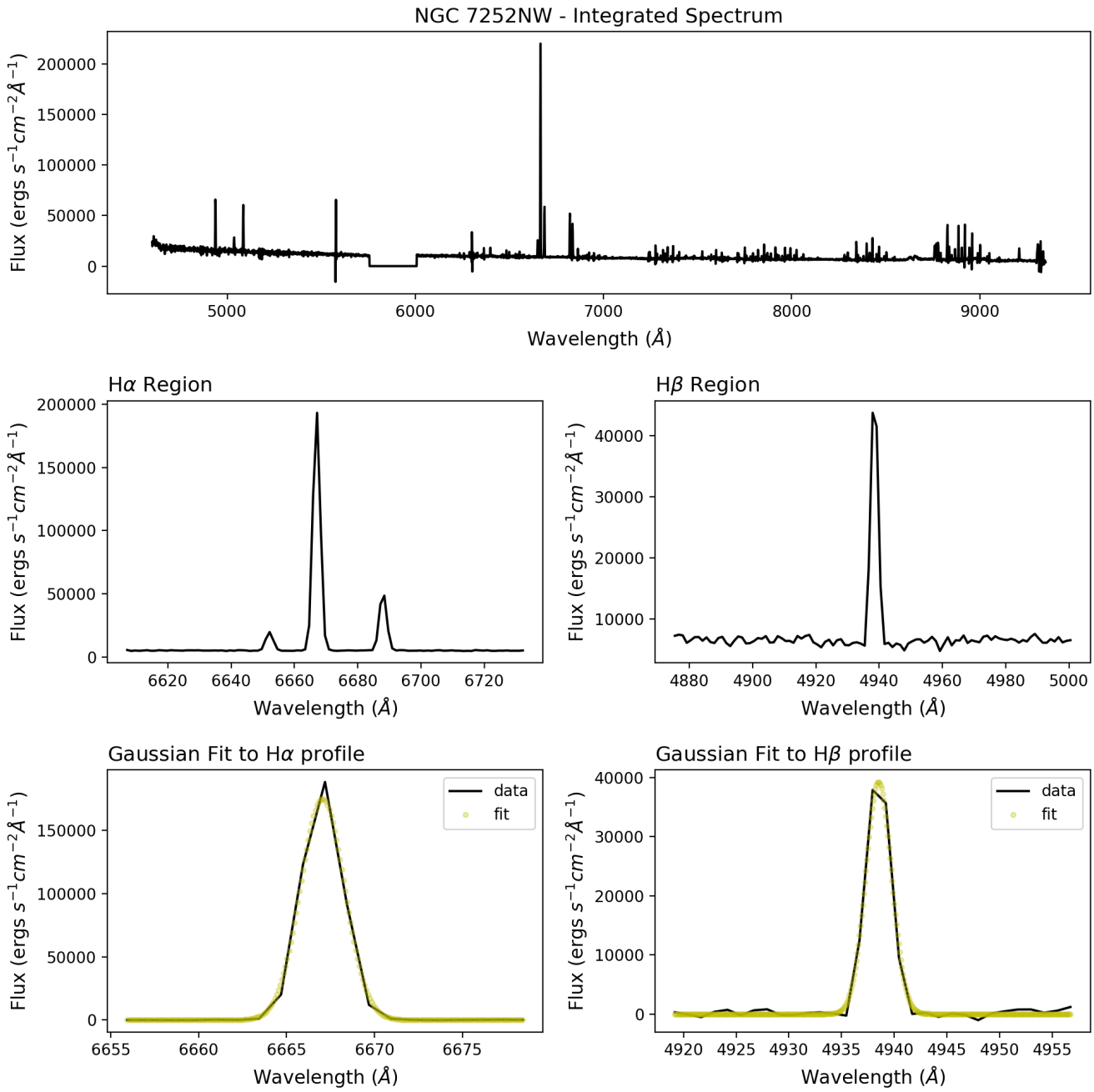

Figure A.2: Analysis on the integrated optical spectrum of NGC 7252NW. Top panel shows the integrated optical spectrum for NGC 7252NW, middle panel displays the regions of interest for this work (Hα and Hβ) and the bottom panel shows the Gaussian fit performed over Hα and Hβ profile, respectively.